Cement and Concrete Research 161 (2022) 106955

Contents lists available at ScienceDirect

Cement and Concrete Research

journal homepage: www.elsevier.com/locate/cemconres

A new four stage model of capillary pressure in early age concrete: Insights from high capacity tensiometers

Armin Jamali *, Joao Mendes, Brabha Nagaratnam, Michael Lim

Mechanical and Construction Engineering, Northumbria University, Newcastle, United Kingdom

ARTICLE INFO

Keywords:
Capillary pressure
High capacity tensiometer
Early age shrinkage
Self-consolidating concrete
Curing duration
Shrinkage reducing admixture

ABSTRACT

Capillary pressure is frequently measured to evaluate the shrinkage performance of concrete but has been limited to pressures <100 kPa preventing a better understanding of the early age factors affecting concrete durability. In this study, high capacity tensiometers (HCTs) were employed for the first time to investigate the behavior of early age concrete. The evolution of capillary pressure in Self-Consolidating Concrete (SCC) with and without shrinkage reducing admixture was evaluated. The results demonstrate that HCTs are capable of measuring capillary pressure beyond 1500 kPa. This transformative new record of capillary pressure behavior has enabled the development of a model for the capillary pressure in early age concrete correlated to water evaporation, self-desiccation, setting time, temperature, and hydration processes. This ability to quantify real-time capillary pressure change in concrete generates important implications for optimizing the commercial durability of SCC and for understanding the link between early age concrete processes and resultant mechanical performance.

1. Introduction

Cracks from plastic shrinkage may form in concrete during the first few hours of the casting, before the final setting time when the concrete is in a plastic or semi-plastic phase and has not gained significant tensile strength [1,2]. Concrete structures with a high surface-to-volume ratio such as pavements, airfields, bridge decks, and slabs for construction are more vulnerable to this phenomenon. Apart from the aesthetic consideration, cracking facilitates the penetration of corrosive elements into the concrete and damages the steel reinforcements leading to a reduction in durability and an increase in the maintenance cost of infrastructures [3–6]. According to a recent report by the UK National Highways, more than £80 M is annually allocated to repair deteriorated concrete pavements in the United Kingdom alone [7]. Since shrinkage is an inherent characteristic of cement paste, and coarse aggregates play a restraining role, concrete containing a higher volume of cement and finer aggregates such as Self-Consolidating Concrete (SCC), Ultra-High-Performance Concrete (UHPC) and, more recently, 3D printing concrete are more prone to cracking due to the shrinkage [8–14].

The mechanism of plastic shrinkage has been widely investigated [3,6,14–19]. The volume reduction in early age concrete is made up of two sequential stages: vertical and horizontal deformation. The former, also known as concrete settlement, generally occurs immediately after casting when it is in its plastic phase until the initial setting time of the concrete. The horizontal deformation generally starts after the initial setting time [3,11,20]. Once the fresh concrete has been cast in a mold, solid particles including aggregates, fillers and cement, which are denser than water, settle due to the gravity and compress the porosities of concrete bulk. During this vertical settlement, the pore solution is pushed upwards and accumulates on the concrete surface, also known as bleeding [14,21,22]. The bleeding water forms a thin layer covering the top surface of the concrete. The thickness of this layer is reduced mostly due to water evaporation following the termination of the bleeding regime. When all bleeding water has been consumed, the concrete surface is exposed to drying and a complex series of menisci are formed inside the capillary pores. Due to surface tension, negative pressure (capillary pressure) builds up in the interconnected pores. As capillary pressure evolves, tensile forces acting on the solid particles lead to a reduction in the volume of the concrete known as a plastic shrinkage. If plastic shrinkage is restrained externally or internally by steel reinforcement, substrates, solid particles, etc., tensile stresses are created that may result in cracking if they exceed the tensile strength capacity of the concrete [3,6,15,18,19,22,23].

Capillary pressure has been identified as the main cause of plastic shrinkage and can be determined by the Gauss-Laplace equation [19] (Eq. 1).

* Corresponding author.
E-mail address: armin.jamali@northumbria.ac.uk (A. Jamali).

https://doi.org/10.1016/j.cemconres.2022.106955
Received 13 April 2022; Received in revised form 23 July 2022; Accepted 19 August 2022
Available online 27 August 2022

$$p_c = -\frac{2\gamma cos\theta}{r} \quad (1)$$

where, capillary pressure, p_c depends on the surface tension of the pore solution, γ (7.28×10^{-2}N/m at 293.15 K for water), contact angle of solid-liquid interface, θ (0° for concrete–water) and the radius of assumed cylindrical pores, r, as shown in Fig. 1.

Self-desiccation and evaporation are considered respectively as the main internal and external factors governing capillary pressure development. Self-desiccation occurs within the concrete when the water to cement ratio is lower than 0.5 and capillary pressure builds up due to the reaction of cement with pore water during the hydration stage. Evaporation is affected by environmental conditions including temperature, relative humidity (RH), wind velocity, and curing regime. Progression of cement hydration and evaporation processes reduce the radii of the menisci resulting in higher capillary pressure and, consequently, plastic shrinkage [11,19,24–26]. The use of shrinkage reducing admixture (SRA) is a method through which the properties of pore water such as surface tension, contact angle, and viscosity, are modified resulting in a reduction in capillary pressure and plastic shrinkage [24,27–33]. The curing regime is another method affecting capillary pressure by controlling the environmental conditions [34]. Slowik et al. [26,35] showed that rewetting of the concrete surface leads to prevention of or delay in the build-up of capillary pressure, which may reduce the plastic shrinkage cracking risk.

Monitoring the capillary pressure development in early age concrete holds significant potential to mitigate plastic shrinkage effects by guiding the development of appropriate (or preventing inappropriate) methods relative to the types of concrete used and relevant environmental conditions. However, direct measurement of capillary pressure in the concrete is challenging. Therefore, indirect methods have been used in the past to infer the capillary pressure development. Li et al. [36], Huang et al. [37] Zhu et al. [38] calculated the capillary pressure values by measuring the pore diameters of the hardened concrete through mercury intrusion porosimetry (MIP) and nitrogen adsorption (NA) analysis. Slowik et al. [19] and Liang et al. [39] also investigated the relationship between the electrical resistivity, moisture distribution and capillary pressure rise in the concrete. However, both approaches are limited by underpinning assumptions, measurement accuracy, inferred values, experiment difficulty, and cost. Pore diameter measurements are also restricted to hardened concrete i.e., not in the plastic or semi-plastic phase.

Capillary pressure in the concrete has been directly measured by the capillary pressure sensors [11,12,19,20,26,40]. However, because of the low capacity of these sensors, capillary pressure measurements have been limited to 100 kPa, a value that is typically reached within the initial few hours after concrete casting. Furthermore, these sensors cease to operate if air entry of the porous filter is reached and cavitation occurs within the water reservoir or there is a blockage of the sensing face by cement paste [6,19,26,41,42]. Given these shortcomings, models developed to predict the capillary pressure value and plastic shrinkage cracking risks based on the evaporation rate, bleeding and settlement, have been limited to concrete ages of about 6 h and have not been validated for longer periods or higher capillary pressures [6,11,14,19,20,40,42]. This is an important limitation because the hydration rate and self-desiccation of cement occurring after 6 h of concrete age are at their highest, causing higher capillary pressures due to the self-desiccation, a process demonstrated by Lura et al. [43] and Poole [44]. Therefore, the capillary pressure values and the proportions of its constituent factors including self-desiccation and evaporation need to be determined during this period in order to develop suitable methods for controlling the plastic shrinkage cracking. Since capillary pressure and its resulting stresses build up in the plastic phase and potentially continue in the semi-plastic and hardened phases of concrete, tracking the capillary pressure for longer periods can explain/reveal how stresses evolve in the phase transition zones i.e., from the plastic shrinkage to the drying shrinkage [45].

High capacity tensiometers (HCT), initially developed by Ridley and Burland at Imperial College London, are devices employed to directly measure the capillary pressure values up to 2000 kPa in soil [46]. HCTs comprise of a ceramic porous filter with an air entry value (AEV) of 1500 kPa, a small water reservoir with a volume of about 3 mm^3, and a pressure transducer with a working similar pressure range of the AEV of the ceramic filter, contained within a stainless steel cylindrical vessel (Fig. 2). Although each component could affect the performance of the HCT, the ceramic filter plays the most significant role. The maximum measurable value of the pore pressure depends on the air entry value of the ceramic filter, which is inversely proportional to its largest pore diameter. To be operational, the HCT ceramic filter and water reservoir need to be fully saturated with deionized deaired water to measure the capillary pressure properly. This is achieved by pre-pressurizing the HCT with pressure controllers, using deionized deaired water at pressures equal to or greater than the AEV of the ceramic filter [47–49].

Although HCTs are commonly used to study the hydromechanical behavior of unsaturated soils, their application to directly measure the capillary pressure in concrete has not been previously investigated. The use of HCTs to directly monitor the capillary pressures in concrete through early age phases has the potential to provide a step-change in research and innovation for construction processes. In this study, the applicability of HCTs to concrete condition monitoring has been investigated. HCT performance under a wide range of capillary pressure values and different curing conditions has been evaluated for SCC with

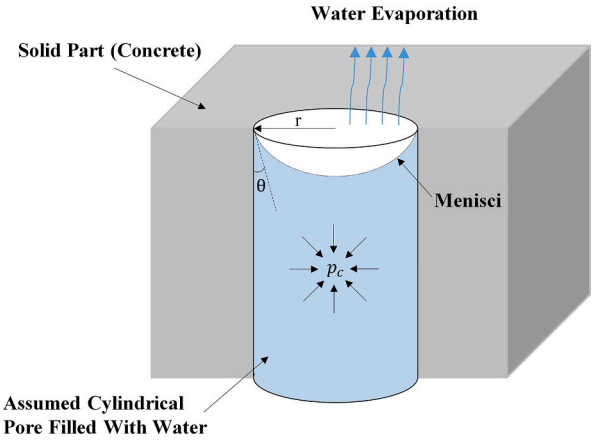

Fig. 1. A schematic view of capillary pressure due to formation of menisci.

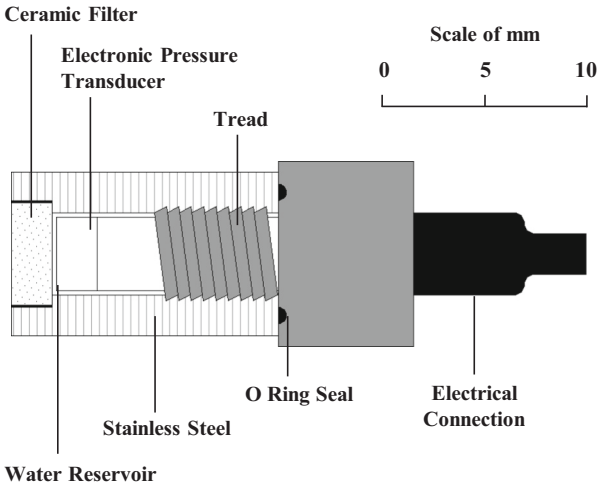

Fig. 2. A schematic view of high capacity tensiometer and its components.

and without SRA. The results have highlighted previously undocumented stages in early age concrete development and have been used to propose a new model for the evolution of capillary pressure in early age concrete. The model proposes different stages based on the changes in the rate of capillary pressure development in different states of early age concrete including plastic, semi-plastic and hardened phases. In this study, determination of bleeding, setting time, mass loss, temperature, hydration degree and microstructure investigation, have been conducted on fresh and hardened concrete to explain the change in the evolution of capillary pressure in different stages.

2. Experimental program

The ability of HCTs to quantify capillary pressure development within mixes with and without SRA under different curing times (8 and 16 h) and without curing have been investigated. In each experiment bleeding, concrete setting times, and capillary pressure along with mass loss and temperature were measured. Isothermal calorimetry tests were also carried out to monitor the hydration process of cement during the experimental program. Furthermore, a time-lapse camera recorded the physical changes visible on the concrete surface during the tests and the changes in porosity of SCC was investigated by Scanning Electron Microscope (SEM).

2.1. Materials and mixture compositions

A high strength cement (Type I) with 52.5 N produced by the Hanson (Middlesbrough, UK) conforming to the requirements of EN 197-1 [50] and BS 8500-2 [51] was used in this study. The chemical, physical, and mechanical properties of cement provided by the manufacturers, are presented in Tables 1 and 2. Crushed gravel from the Wensley quarry (Leyburn, UK) with the maximum nominal grain size of 14 mm was used as a coarse aggregate. Two types of sands, including silica sand from the Cheviot quarry (Wooler, UK) and rock sand from the Harden quarry (Rothbury, UK) with a size range of 0 to 4 mm, were used as fine aggregates. The properties of the aggregates used are shown in Table 3. A polycarboxylic ether-based superplasticizer was used to increase flow ability of SCC. Mapecure SRA-25, produced by MAPEI S. p. A., was used as shrinkage reducing admixture. The properties of SRA are shown in Table 4.

Table 5 shows the mixture compositions of SCC with and without SRA. The letters “C” and “S” refer to the control mixes and the mixes with SRA, respectively, and the codes 0 h, 8 h and 16 h refer to duration of sealed curing time in hours. The cement content and water to cement ratio were 480 kg/m^3 and 0.4, respectively. The volumetric portions of cement and aggregates were identical for all mixes. To prepare the mixes, dry aggregates were premixed for 2min in a Mini 130 Altrad Belle mixer. Afterwards, the cement was added to the aggregates and mixing continued for 2min. Three quarters of the mixing water and superplasticizer (and SRA) were then added gradually to the mixture and mixing continued for 3 min. The materials stuck to the inner walls of the mechanical mixer were then added to the mixture by scraping while the remaining water was also added, and mixing resumed for another 2 min. The workability of mixes was measured according to BS EN 12350-8 [52]. The time to reach 500 mm diameter (T_{500}) and the final diameter are 4 s and 620 mm respectively. To measure the specific gravity of the SCC, a steel cylinder mold with dimensions of 100 × 200 mm was filled with the fresh SCC and weighed. The density of the fresh mixes was determined to be 2367 kg/m^3.

Table 2
Physical and mechanical properties of cement.

Specific surface (m^2/kg)	Density (kg/m^3)	Normal consistency (%)	Initial setting time (min)	Compressive strength at 28 days (MPa)
420	3100	28	170	59.5

Table 3
Properties of aggregates.

Aggregates	Quarry	Maximum size (mm)	Specific gravity (SSD) (g/cm^3)	Water absorption (%)
Gravel	Wensley	14	2.59	0.5
Silica sand	Cheviot	4	2.54	1.7
Rock sand	Harden	4	2.58	1.1

Table 4
Properties of SRA.

Consistency	Color	Density (g/cm^3)	pH
Liquid	Light amber	1.0 ± 0.030	8 ± 1

2.2. Capillary pressure

In this study, 6 HCTs specifically developed for testing early age concrete were designed and assembled at Northumbria University. These new sensors were employed to measure the capillary pressure of the mixes, as shown in Fig. 3. These new HCTs consists of a 1500 kPa AEV ceramic filter, 50 mm^3 water reservoir and a thermally compensated (in the range of 16 to 71 °C) Omega PX61V1 pressure transducer with a pressure range of 2000 kPa or 6000 kPa. Prior to use, the HCTs were kept inside stainless steel saturation vessels pressurized with deaired deionized water at 3 MPa, using a 4 MPa pressure-volume controller from GDS instruments Ltd. (Fig. 4). During testing, three HCTs were removed from the saturation vessel 2 h before the start and put immediately in deionized water to prevent cavitation and to reset the pressure reading to 0 kPa. A protective tube with a similar diameter to the HCT (25 mm) and a height of 100 mm was placed on the top of each HCT and sealed with electrical tape to avoid penetration of water into the electrical parts of HCT during the test. Measurement of capillary pressures with HCTs is achieved by placing the HCT in contact with a porous material (soil, concrete, etc.). When the ceramic filter is in contact with the pore water in the porous material, the pore pressure will draw the water out from the filter and the HCT reservoir as a result of the pressure difference. This depressurization leads to a deflection of the membrane connected to the strain gauge in the HCT that will continue until equilibrium. When the capillary pressure exceeds the working range of the HCT, cavitation occurs through the emergence of air bubbles inside the water reservoir, which can be detected by a sudden drop in the measured capillary pressure to about 100 kPa of relative pressure (0 kPa absolute pressure at sea level) [47–49].

After casting the 100 mm cubic specimens, the samples were transferred to a controlled environment with a temperature of 22± 2 °C and relative humidity of 50 ± 4 %. Each HCT was placed in the center of a cubic sample to a depth of 50 mm and connected to the data logger system recording capillary pressure values at 5 s intervals. To measure the change in the internal temperature of the concrete specimens, a K-type thermocouple was embedded at a depth of 50 mm in each sample,

Table 1
Chemical composition of cement (%).

SiO_2	Al_2O_3	Fe_2O_3	CaO	MgO	SO_3	K_2O	Na_2O	Cl	C_3S	C_2S	C_3A	C_4AF	Insoluble residue
19.78	4.80	2.84	64.75	1.18	3.14	0.57	0.24	0.05	63.8	11.9	8.6	6.5	0.63

Table 5
Mixture composition of concrete.

Mix code	Curing time (h)	Cement (kg/m^3)	Water (kg/m^3)	Gravel (kg/m^3)	Coarse sand (kg/m^3)	Fine sand (kg/m^3)	SRA, weight of cement (%)	Super-plasticizer (kg/m^3)
C-0 h	0	480	192	795	265	668	0	2.3
C-8 h	8	480	192	795	265	668	0	2.3
C-16 h	16	480	192	795	265	668	0	2.3
S-0 h	0	480	192	795	265	668	1.5	2.3
S-8 h	8	480	192	795	265	668	1.5	2.3
S-16 h	16	480	192	795	265	668	1.5	2.3

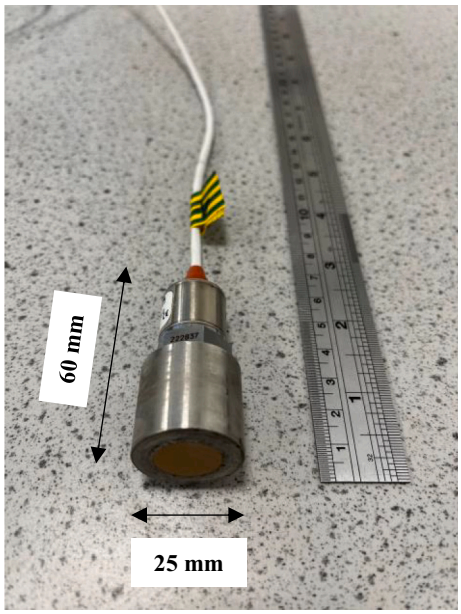

Fig. 3. HCT used in this study.

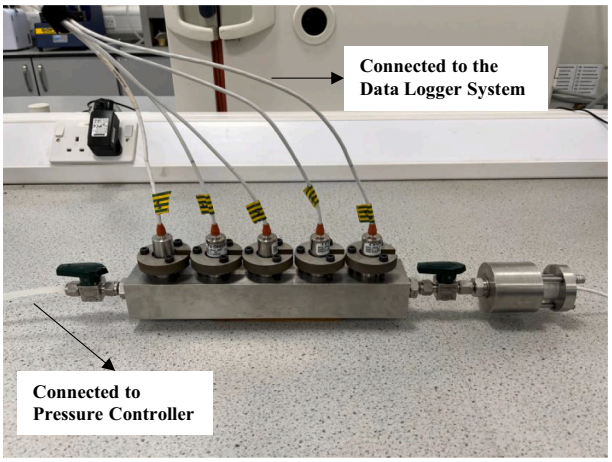

Fig. 4. HCTs under 3 MPa water pressure in the steel vessels.

recording the temperature value every 5 s. After placing the HCTs and thermocouples, the top surfaces of samples with 8 and 16 h curing times were covered with polyethylene sheets and sealed with elastic bands in order to prevent evaporation and to provide the determined initial curing condition with the relative humidity at least 95 %. To determine the rate of water evaporation, one of the concrete specimens was placed on a balance during the test and its mass loss was also recorded at intervals of 5 s to an accuracy of 0.1 g. Three specimens were fabricated for each set of tests including capillary pressure, temperature and mass loss, and the calculated average was reported as the final results. A schematic view and a picture of the test are illustrated in Fig. 5.

2.3. Bleeding

The bleeding tests were conducted according to ASTM C232 [53]. To provide a similar condition to the capillary pressure tests and to prevent any effect of collecting bleeding water on the capillary pressure measurements, fresh concrete was placed in three cubic molds (100 mm) separated from the capillary pressure samples. Specimens were wrapped with a polyethylene sheet to prevent evaporation and placed in the same environmental condition at a temperature of 22 ± 2 °C and relative humidity of 50 ± 4 %. The tests were carried out on a leveled surface free of any vibrations. To draw off the bleeding water, samples were uncovered at the time of collection and accumulated water on the top surface of the specimens was collected by a pipet at intervals of 10 min during the first hour after casting. Afterward, the measurement was continued every 30 min until bleeding of water stopped. A plywood block with a thickness of 30 mm was also placed under the corner of a sample at 2 min before each collection time to facilitate the accumulation of water.

2.4. Setting time

The initial and final setting times of the mixes were determined based on penetration resistance in accordance with ASTM C403 [54]. To obtain the mortar representative of the studied mixes, fresh concrete was passed through a 4.75 mm sieve and cast in three cylindrical molds (height 50 mm and diameter 110 mm). Specimens were placed in the same environmental condition (at a temperature of 22 ± 2 °C and relative humidity of 50 ± 4 %) and those with 8 and 16 h curing time were covered with polyethylene sheet. Two hours after adding the water to the mixture (cement), the tests to determine the initial setting time were conducted and continued at intervals of 30 min until the final setting time. The initial and final setting times were defined when the needle penetrated 25 mm into the mortar within 10 s under pressures of 3.5 MPa and 27.6 MPa, respectively.

2.5. Isothermal calorimetry test

The isothermal calorimetry method is used to quantify the development of cement hydration which is also known as the hydration degree. The values usually range between 0 (no hydration) and 1 showing the completed hydration process [44]. Given that the reaction of cement with water is an exothermal process, hydration degree might be proportional to the heat flow [55]. The hydration degree at time t is considered the ratio of amounts of heat developed up to the time t to the total heat expected, as indicated in Eq. 2 [56–58]:

$$\alpha_{(t)} = \frac{H_{(t)}}{H_{Cem}} \tag{2}$$

where: $\alpha_{(t)}$ = degree of hydration, $H_{(t)}$ = the amount of heat which has been evolved up to time t (J/g), and H_{Cem} = the total amount of heat which is available (J/g).

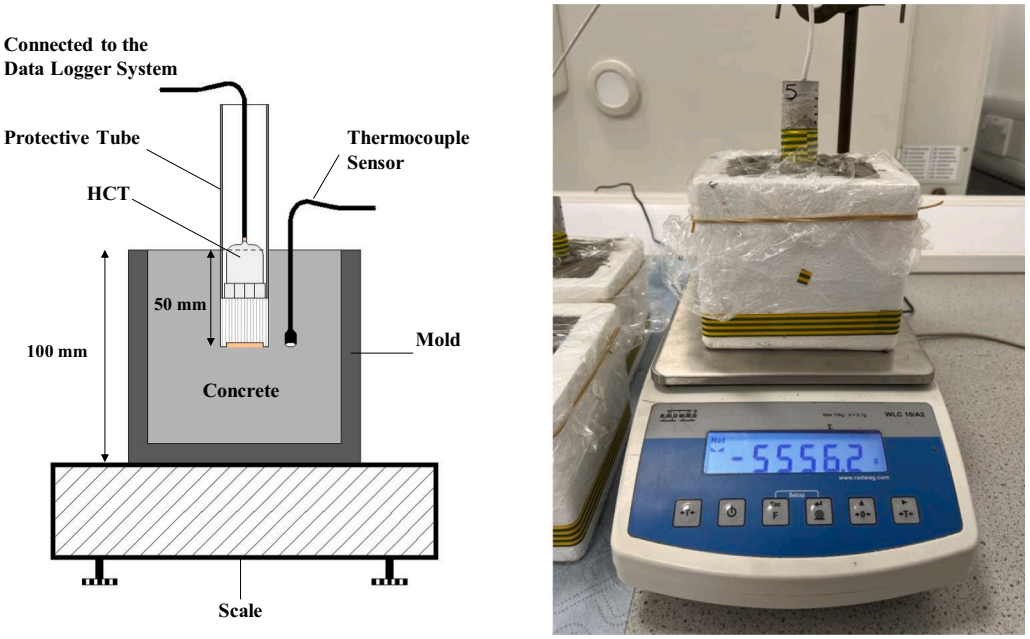

Fig. 5. (a) A schematic view and (b) an actual image of the capillary pressure test specimen under curing condition.

In this study, the isothermal calorimetry method was used to measure the heat developed during the test due to cement paste hydration, $H_{(t)}$. Calorimetry measurement was performed on 4.2 g of cement paste including 3 g of cement and 1.2 g of water (w/c = 0.4). Three glass ampoules were filled with the cement paste and placed in the microcalorimeter (TAM air, TA Instruments) with a fixed temperature of 20 °C. The heat flow was recorded with intervals of 5 s for 24 h.

The total amount of heat due to hydration of cement, H_{Cem}, at $\alpha = 1$ is a function of chemical compositions of used cement which can be calculated by Eq. 3 [59]:

$$H_{Cem} = 500 \bullet P_{C_3S} + 260 \bullet P_{C_2S} + 866 \bullet P_{C_3A} + 420 \bullet P_{C_4AF} + 624 \bullet P_{SO_3} + 1186 \bullet P_{FreeC_a} + 850 \bullet P_{MgO} \quad (3)$$

where P_i is the portion of each component (%) in cement presented in the Table 1.

2.6. Time-lapse monitoring

To achieve conformity between the period of each state determined by the experimental program and changes in the surface of concrete, a time-lapse camera was employed. To monitor the change in the surface of the specimen exposed to drying, a time-lapse camera was installed on top of the sample. A Canon Rebel XS (1000D) camera with a resolution of 10.5 megapixels as set to capture the top surface of the sample in macro mode and set to take a snapshot at an interval of 15 min.

2.7. SEM imaging

To investigate the effect of curing duration on the capillary pressure, the microstructure of SCC including the determination of pore diameter distribution and hydration products were investigated by scanning electron microscope, Oxford Instruments. After 24 h from casting, small samples with dimensions of 10 mm were cored from the capillary pressure cubic specimens. Since samples need to be electrically conductive for SEM imaging, they were coated with copper tapes, silver solution and platinum, and were immediately placed in the chamber of microscope.

3. Results and discussion

3.1. Validation of HCTs' results

To evaluate the repeatability and consistency of the results obtained by different HCTs, 6 cubic samples were fabricated from the same concrete batch and each HCT was used to measure the capillary pressure of each sample separately. All samples were under 16 h sealed curing (C-16 h) and the same environmental conditions as mentioned previously.

The capillary pressure evolution recorded by the HCTs, presented in Fig. 6, shows that HCTs are capable of measuring both types of pore pressure (positive pore pressures, also known as hydrostatic, and negative pressures or capillary pressure). The start of the measurement of the evolution of pore pressure coincides with the installation of the HCTs in the concrete samples. The build-up of capillary pressure of all C-16 h specimens started in a short period (about 20 min) from $t = 4.6$ to $t = 4.9$ h after casting and the evolution of capillary pressure was monitored until the HCTs were not able to monitor further capillary pressure, i.e., cavitation occurred in the HCTs as aforementioned. Although the cavitation time of HCTs varied between 15 and 19 h, the capillary

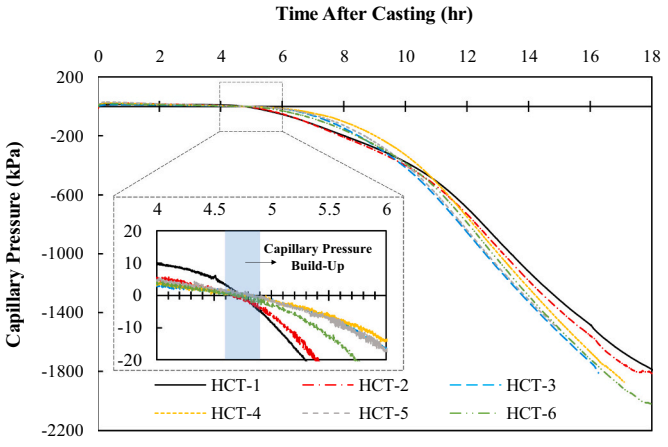

Fig. 6. Capillary pressure value of the C-16 h measured by 6 different HCTs.

pressure measured by all HCTs showed similar trends and values over the monitoring period. It is worthwhile to mention that the difference in cavitation time of HCTs is possibly related to the relocation of existing air bubbles in the ceramic filter, resulting in cavitation at higher or lower values than the nominal air entry value of the HCT ceramic filter [47–49]. The average linear rate of capillary pressure evolution during the test was −111 kPa/h and the standard deviation was 7.59 kPa/h, which is 7 % of the average rate. This validates the novel application of HCTs for monitoring the evolution of capillary pressure in early age concrete. Furthermore, the results of capillary pressure evolution in separate identical specimens indicate that the gradient of capillary pressure evolution might be considered as a property of mixes at the same depth regardless of the size and distribution of pores.

Moreover, as illustrated in Fig. 6, it is interesting to mention that the capillary pressure values, measured by each HCT placed at the same depth in each separate specimen, are almost similar (±5 % of average value). These results suggests that the diameter of the HCT ceramic filter (15.2 mm) is large enough as to contact the nearly whole range of interconnected pores enabling the measurement of the existent pore pressure in the concrete. The details of the HCTs used in the experimental program and obtained results are summarised in Table 6.

3.2. Capillary pressure evolution in early age concrete model

The evolution of capillary pressure in the control mix without curing is shown in Fig. 7. Four distinct stages can be identified based on the gradient of the capillary pressure evolution measured by the HCTs. Interpretation of these stages was based on the correlation of capillary pressure evolution with mass loss, internal temperature, and hydration degree, illustrated in Fig. 7 and Fig. 8 respectively, and the qualitative information from the time-lapse imagery.

3.2.1. Stage 1

From casting to the initial setting time ($t = 2.5$ h) and consequently the end of the bleeding phase ($t = 2.75$ h), no capillary pressure was observed in the SCC. During this time, the surface of the samples was covered by a thin layer of water during the settlement as shown in Fig. 9a, preventing the formation of menisci and capillary pressure due to evaporation. As can be seen in Fig. 8, the hydration of the cement paste was dormant and the degree of hydration was $\alpha_{(t=2.75)} = 0.7\%$, resulting in a lack of self-desiccation and, in turn, capillary pressure. During this stage, sustained solid particles in the pore water applies gravitational forces to the water resulting in a positive (hydrostatic) pressure of about 40 kPa in the pore water. Similar results were reported by Schmidt and Slowik [41] and Ghourchian et al. [60]. Eq. 4 determines the hydrostatic pressure undergone by pore fluid due to the self-weight of the solid particles when bleeding stops [21].

$$\psi_p = \rho_f g(h - z) \tag{4}$$

where ψ_p is the potential of pore fluids' pressure (Pa), ρ_f is the specific weight of the pore fluid (kg/m^3), g is the acceleration of gravity (m/s^2), h is the height of the sample (m) and z is the distance to the bottom of the sample (m).

Table 6
The properties of high capacity tensiometer used in this study.

HCT	Pressure transducer range (kPa)	AEV of ceramic filter (kPa)	Maximum measured capillary pressure (kPa)
HCT 1	2000	1500	−1804
HCT 2	2000	1500	−1811
HCT 3	2000	1500	−1994
HCT 4	6000	1500	−1882
HCT 5	2000	1500	−1519
HCT 6	6000	1500	−2026

3.2.2. Stage 2

A reduction in the thickness of the thin water layer (Fig. 9b) following bleeding stop results in a series of menisci in the pores close to the concrete surface resulting in the development of capillary pressure, see Fig. 7. With increasing mass loss due to evaporation, the curvature of the menisci increases leading to increase of capillary pressure values at a rate of −33.5 kPa/h until the final setting time of concrete at $t = 5$ h (as shown in Fig. 9c). In this period, because of the low hydration degree, $\alpha_{(t=5)} = 2.6\%$, evaporation is the dominant factor for the change in capillary pressure. A similar trend was observed in this timeframe in previous studies [11,14,19,40,41,60].

3.2.3. Stage 3

After the final setting time of the SCC ($t = 5$ h), water curvature increased leading to the development of capillary pressures at a higher rate of about −74.3 kPa/h. The rate of temperature change (Fig. 7) and heat flow (Fig. 8), which are proportional to the degree of hydration of the cement paste, continued to increase with a slightly steeper rate up to $t = 10.7$ h. The degree of hydration at the end of this stage, $\alpha_{(t=10.7)}$, was determined about 13.5 % indicating higher self-desiccation. The water loss due to self-desiccation and evaporation led to capillary pressure falling at a steeper rate compared to the previous stage.

3.2.4. Stage 4

When the internal temperature evolution of SCC leveled off before the highest point (about 23 °C at 10.7 h), the rate of heat flow reached its peak. Afterward, although the rate of heat flow reduced slightly up to $t = 18$ h, it still experienced a high rate resulting in an increase in degree of hydration from $\alpha_{(t=10.7)} = 13.5$ % to $\alpha_{(t=18)} = 26.5$ % (as seen in Fig. 7 and Fig. 8 respectively). An increase in hydration processes in this stage lead to a greater level of self-desiccation (Figs. 7 and 9d). Self-desiccation appears to be the dominant factor of capillary pressure evolution in this stage, as the rate of mass loss reduced about 30 % compared to Stage 3. The capillary pressure developed at a higher rate of about −173.4 kPa/h during this period in comparison with the previous stage. As a result, concrete undergoes more critical loss of water and further desaturation degree of the pores.

3.3. The effect of curing time on the capillary pressure

3.3.1. SCC without SRA

The effect of duration of sealed curing on the capillary pressure, mass loss and temperature of SCC without SRA are shown in Fig. 10 and Fig. 11, respectively. Following the proposed conceptual model in Section 3.2, all mixtures experienced a positive hydrostatic pressure up to the end of bleeding phase at around $t = 3$ h, i.e., in Stage 1, and no capillary pressure was observed because of the bleeding regime while pores remain fully saturated.

In the second stage, capillary pressure built-up was observed for C-0 h around the final setting time ($t = 5$ h) due to evaporation of water and the start of pore desaturation. Whereas, for mixes with 8 h and 16 h curing durations, capillary pressure remained unchanged until their final setting time ($t = 4.75$ h). The observed difference in capillary pressure build-up after the bleeding regime had ceased in mixes with sealed curing time (C-8 h and C-16 h) can be attributed to the development and entrapment of moisture between the top surface of the samples and polyethylene sheet (resulting in an environment close to 100 % of relative humidity), which coupled with the negligible degree of hydration, resulted in the prevention of capillary pressure build-up during Stage 2.

In the third stage, capillary pressure in all mixes developed at a similar rate of about −70 kPa/h up to $t = 8$ h. At the start of this stage, the capillary pressure value of C-0 h was twice as high as that of C-8 h and C-16 h because of the earlier exposure to drying which led to a higher loss of capillary water, which also explains the significant difference between the rate of mass loss of mixes with and without sealed

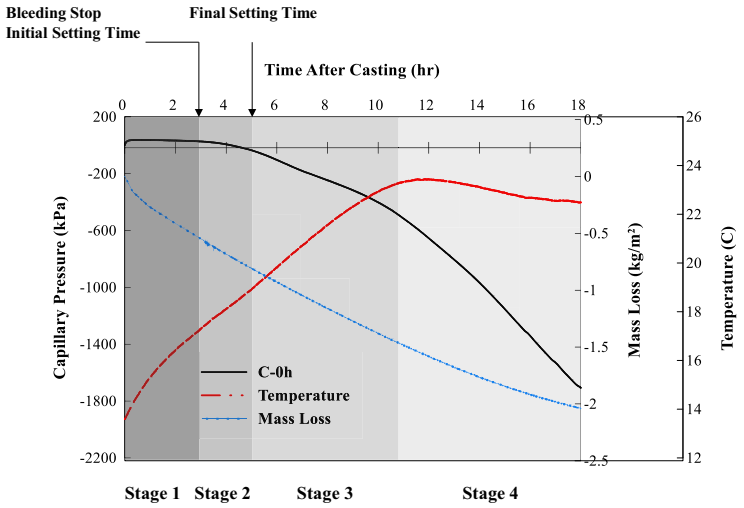

(a)

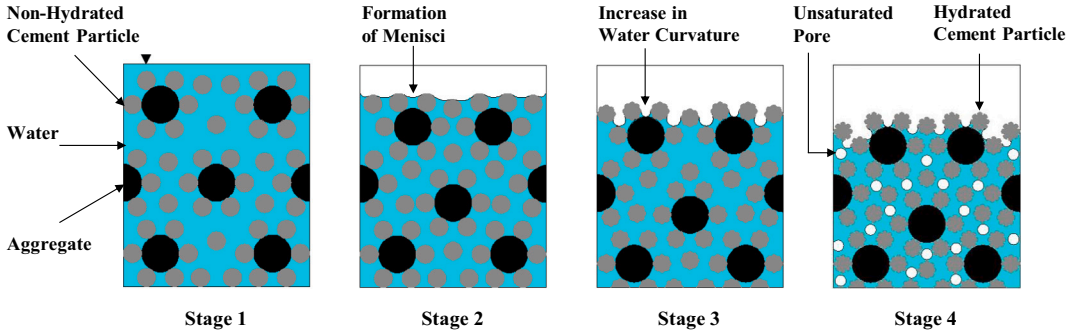

(b)

Fig. 7. (a) The correlation between capillary pressure behavior, mass loss, internal temperature, bleeding, initial and final setting time of SCC without curing, (b) Schematic stages of capillary pressure evolution.

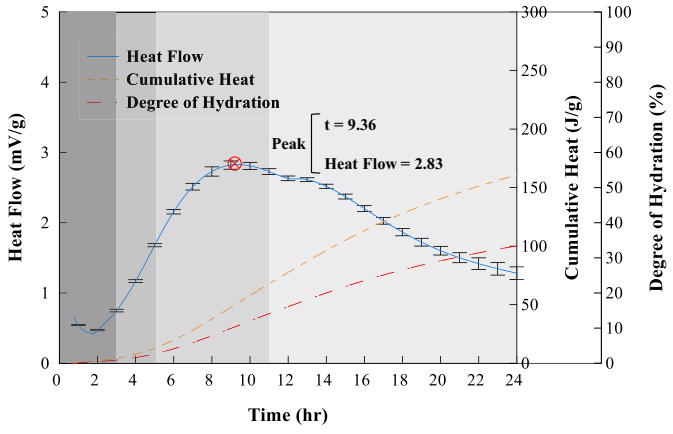

Fig. 8. The rate of heat and cumulative heat evolved per gram of cement with w/c = 0.4 at 20 °C.

curing, as illustrated in Fig. 11a. The fact that an identical capillary pressure rate was initially observed in all mixes suggests that another factor contributed to capillary pressure development in the absence of mass loss due to evaporation in mixes with sealed curing. The capillary pressure development observed in mixes with sealed curing could be due to self-desiccation as a result of which these mixes experienced a similar evolution rate to the mix without curing in this period. In fact, by increasing the curing duration, the rate of temperature change increased from 0.88 °C/h to 1.93 °C/h (about 120 %) between $t = 5$ h and 8 h, as shown in Fig. 11b. Given that the rate of temperature change is proportional to the heat flow, this increase resulted in a higher degree of hydration and consequently self-desiccation for the mixes with curing in this period [61]. Furthermore, as shown in Fig. 11b, the C-8 h and C-16 h mixes experienced the peak of the heat flow earlier and at higher values than the C-0 h mix leading to the higher self-desiccation to be longer in duration. For the C-8 h mix, after 8 h, i.e., termination of sealed curing, the capillary pressure developed with a steeper rate until around $t = 9.3$ h, which is hypothesized to be the result of the couple effect of higher self-desiccation and further drying that the mixes endure during Stage 3 [62]. On the other hand, the capillary pressure of C-16 h continued with the same rate until around $t = 10.2$ h, i.e., peak of temperature.

In the fourth and last stage, the capillary pressure of mixes with 8 h and 16 h curing durations evolved with a similar rate of about −208 kPa/h, which was higher than that of C-0 h mix (−173.4 kPa/h) until $t =$ 16 h. At $t = 16$ h, the value of capillary pressure for the C-8 h mix was −1781 kPa, which was higher than that of C-16 h (−1556 kPa). The higher self-desiccation in C-16 h, due to a longer curing duration, contributed for the rate of capillary pressure development of C-16 h mix

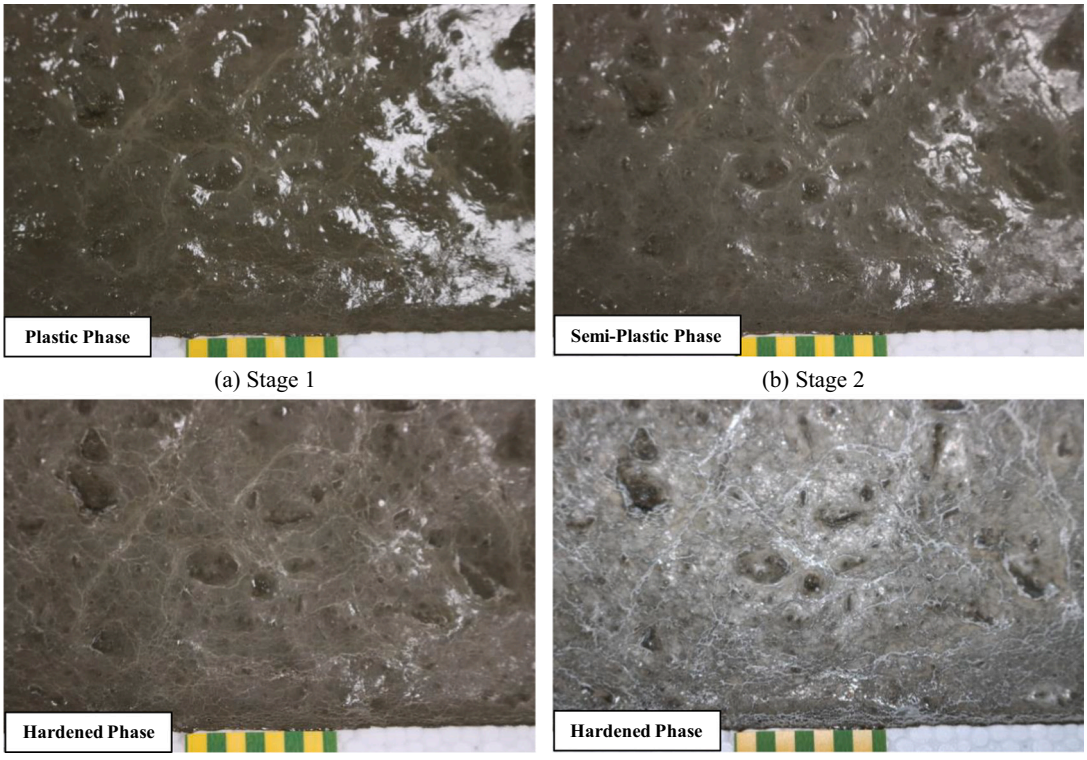

(a) Stage 1 (b) Stage 2

(c) Stage 3 (d) Stage 4

Fig. 9. (a) The change in the surface of the samples at the start of each stage, $t = 0$ h Stage 1, (b) $t = 2.75$ h Stage 2, (c) $t = 5$ h Stage 3, and (d) and $t = 10.7$ h Stage 4.

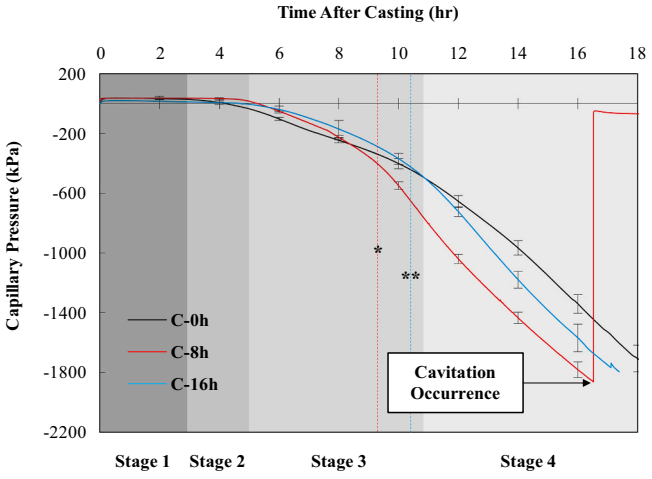

* The start of Stage 4 for the C-8h mix.
** The start of Stage 4 for the C-16h mix.

Fig. 10. The effect of curing duration on the capillary pressure of SCC without SRA.

to be similar to the C-8 h, even in the absence of mass loss due to drying. The observed difference between the capillary pressure value of the C-8 h and C-16 h at $t = 16$ h, was the result of the amount of capillary water available. While in the C-8 h mix, the capillary water dried out due to shorter curing period, in the C-16 h mix, capillary water remained in the pores that progressively changed to chemically and physically bounded water [55]. The longer curing duration in the C-16 h mix also resulted in an increase of the specific surface of the hydrated cement particles as indicated in Fig. 12a which led to higher adsorption of capillary water. By increasing the thickness of physically bound water, the value of disjoining pressure also increases resulting in the compensation of the capillary pressure [55,63].

As shown in Fig. 10, comparatively with the mix without curing (C-0 h), the capillary pressure value and rate for the C-16 h mix were higher. The observed difference can be attributed to the increased proportion of hydrated cement particles, i.e., higher self-desiccation, for the C-16 h mix along with the resulting finer pore size distribution. As it can be observed, comparing Fig. 12a and b it is evident that the longer curing duration resulted in a finer pore size distribution for the mix with longer curing time (C-16 h), where a reduction of about 30 % of pore diameter was observed corroborating the obtained results reported by Samouh et al. [55] and Oliveira et al. [10]. Furthermore, the resulting finer pore size distribution also reduced the permeability within the concrete impeding the distribution of water in unsaturated pores leading to the development of further critical capillary pressure, particularly due to self-desiccation.

The statistical significance of the obtained results presented in Fig. 10 was evaluated through Friedman and Kruskal-Wallis tests in each stage of the plots using the GraphPad 9.3.1 program. The results indicate that in most stages the results between the control mixes including (C-0 h vs. C-8 h, C-0 h vs. C-16 h, C-8 h vs.C-16 h) are statistically significant with *P*-values lower than 0.0001. The only observed exception was with the C-0 h vs. C-16 h in Stage 2 where the Friedman test shows that the results were evaluated as non-significant. Although the results for C-0 h and C-16 h in Stage 2 are different in value, the obtained average is similar for this period resulting in the Friedman test to evaluate the obtained results as being non-significant. Further details for the different stages of capillary pressure evolution in SCC under different curing durations are presented in Table 7.

3.3.2. SCC with SRA

The effect of curing duration on the capillary pressure evolution,

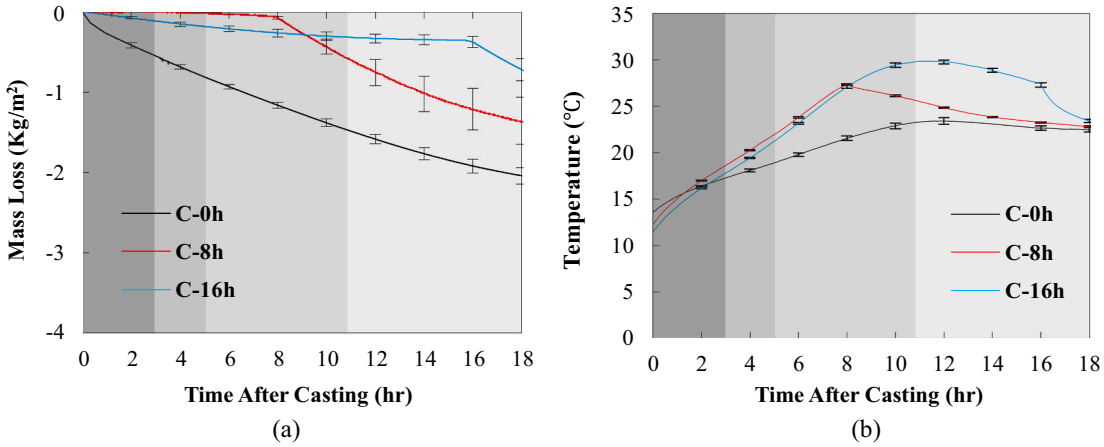

Fig. 11. (a) The effect of curing duration on mass loss, and (b) temperature of SCC without SRA.

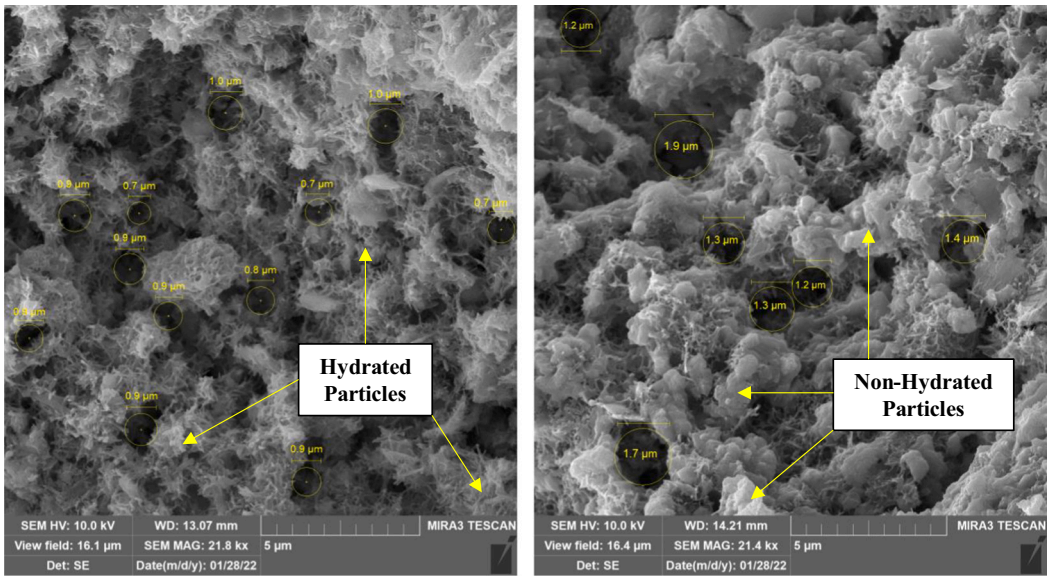

Fig. 12. (a) SEM images showing the microstructure of SCC including cement particles and pores for C-16 h, and (b) C-0 h at the age of 24 h after casting.

mass loss and temperature of SCC with 1.5 % dosage of SRA is illustrated in Fig. 13 and Fig. 14. The results indicate that the use of 1.5 % of SRA reduced the values of capillary pressure by about 70 %. The surfactant particles of the SRA reduced the surface tension of the pore water resulting in a significant reduction in capillary pressure of concrete at an early age [29]. Overall, unlike the control mixes, the capillary pressure rates and values of SCC containing SRA were reduced by longer curing duration up to the age of 18 h. All mixes experienced hydrostatic pressure of 30 kPa in the first stage up to $t = 3.5$ h. Afterwards, the capillary pressure of the S-0 h mix increased at the rate of −10 kPa/h because of the higher rate of evaporation (as seen in Fig. 14a). The mixes with sealed curing, continued to experience a positive pressure in the second stage up to $t = 5$ h due to the prevention of evaporation and low hydration degree. As indicated in Fig. 14b, SRA reduced the rate temperature rise which is proportional to the evolution of heat flow. Indeed, SRA contributed to the reduction in the alkalinity of the pore solution

Table 7
Details of the different stages in capillary pressure of SCC under different curing durations.*, **

Mix code	Bleeding termination (h)		Setting time (h)				Maximum temperature		Starting time of stages (h)		
	Time	St.dev.	Initial	St.dev.	Final	St.dev.	Value (°C)	Time (h)	Stage 2	Stage 3	Stage 4
C-0 h	2.75	0.35	2.5	0.2	5	0.3	23.4	11.9	2.76	5	10.7
C-8 h	2.75	0.35	2.25	0.35	4.75	0.28	27.4	8	–	4.8	9.3
C-16 h	2.75	0.35	2.25	0.35	4.75	0.28	29.9	11.1	–	4.8	10.2
S-0 h	3.25	0.2	3	0.35	5.25	0.2	24.3	14.14	3.5	5	13
S-8 h	3.25	0.2	2.75	0.2	5	0.33	24.4	12.18	–	5.1	11
S-16 h	3.25	0.2	2.75	0.2	5	0.33	30	13.5	–	5.1	11.5

* The time presented in the table is considered after casting.
** Since the bleeding, initial and final setting time were terminated before 8 h, their results are identical for mixes with 8 and16 h curing time.

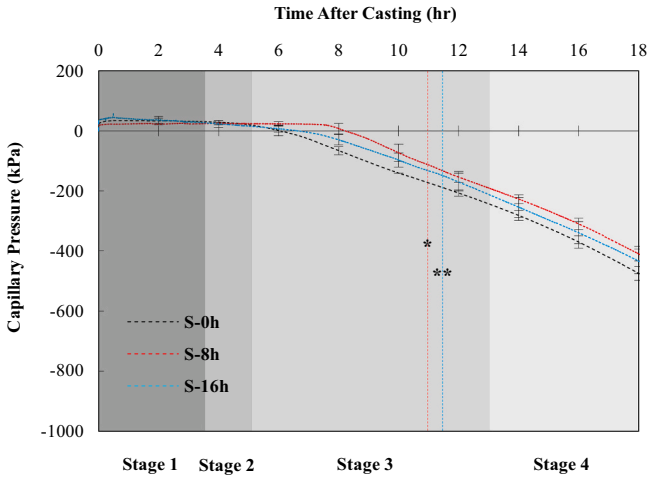

* The start of Stage 4 for the S-8h mix.
** The start of Stage 4 for the S-16h mix.

Fig. 13. The effect of curing duration on the capillary pressure of SCC with SRA.

and could reduce the hydration process and self-desiccation in the SCC [64].

The third stage started for all mixes around $t = 5$ h in which capillary pressure of S-0 h evolved with the higher rate of about −35 kPa/h up to $t = 13$ h due to the coupling effect of evaporation and self-desiccation. Similar to the capillary pressure behavior of control mixes in Stage 3 up to $t = 8$ h, S-0 h experienced a higher capillary pressure value than the mixes with sealed curing due to earlier exposure of drying. The capillary pressure of mixes with sealed curing also developed with the steeper rate of about −12 kPa/h due to a higher hydration degree than the previous stage up to t = 8 h. After the termination of sealed curing for S-8 h, this mix underwent a lower capillary pressure value but at a similar rate (−40 kPa/h) relative to the S-16 h mix up to around $t = 11$ h, when the temperature leveled off for the S-8 h mix. Previous studies showed that the performance of SRA depends on the concentration of SRA in the pores which is related to the pore dimension and its saturation degree [10,31,33]. Rahoui et al. [33] reported that the SRA has better performance in the pores with the saturation degree in the range of 33 % to 77 % because SRA cannot be adsorbed by cement paste in the saturation condition. These findings confirm the higher capillary pressure value of S-16 h relative to the S-8 h in Stage 3. In the last stage, although the rate of capillary pressure development in all mixes increased by about 25 % due to further hydration and drying, the differences between the capillary pressure values remained unchanged. *P*-values lower than 0.0001 for all stages obtained from the Friedman and Kruskal-Wallis tests also confirmed that the results of mixes with SRA including (S-0 h vs. S-8 h, S-0 h vs. S-16 h, S-8 h vs. S-16 h) are statistically significant.

It is important to note that the capillary pressure values in mixes with and without SRA under identical curing duration show that there is a significant reduction of capillary pressure in SRA concrete when longer curing durations are used. A longer curing time and further hydration progress of cement paste increased the proportion and specific surface area of hydrated cement particles resulting in further adsorption of SRA molecules on pore walls. Thus, SRA forms hydrophobic paths through which mixes with longer curing time experience a further reduction in capillary pressure [33]. This finding enhances the effectiveness of SRA in finer and semi-saturated porosities and needs to be considered in design codes and construction projects to increase durability and optimize maintenance costs.

4. Conclusion

In concrete slabs, the plastic shrinkage phenomenon can lead to early age cracking and reduce the long-term durability of structures. Capillary pressure is the main cause of plastic shrinkage, monitoring it through early age development and determination of distinct stages and dominant causes, including evaporation and self-desiccation, gives new insights how plastic shrinkage might be mitigated. In light of these findings and to mitigate capillary pressure effects in early age concrete, the following conclusions and recommendations can be drawn.

- The use of high capacity tensiometers (HCTs) is an exciting new method to monitor the capillary pressure values within concrete up to 2000 kPa, enabling the examination of processes occurring throughout the early age evolution. The HCT approach provides a step-change in the length of measurement achievable, including the plastic phase and the hardened phase, although this can vary depending on the type of concrete and environmental conditions. These transformative data and measurement method could be used as a new reference for the proposed poromechanical models to determine the capillary pressure in concrete and other composite materials.
- When co-located within control mixes, the capillary pressure values measured by different HCTs were highly consistent (within 5 %), validating the use and reproducibility of HCTs for monitoring the evolution of capillary pressure in early age concrete. Regardless of pores' size and distribution, the results also show that the rate of

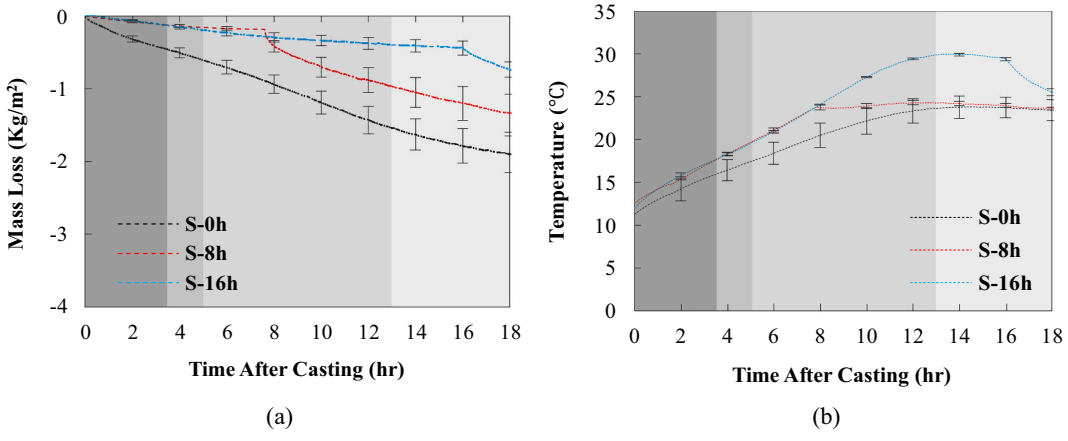

Fig. 14. (a) The effect of curing duration on mass loss, and (b) temperature of SCC with SRA.

capillary pressure evolution might be considered a property of concrete.

- The data presented here allow the development of a new model for describing the evolution of capillary pressure evolution in early age concrete. This new four stage model, governed by bleeding and setting time (stages 1 and 2), evaporation (stages 2–4), and self-desiccation (stages 3 and 4), identifies a dominant factor in each stage of capillary pressure evolution. It is now possible to develop appropriate methods to mitigate the early age shrinkage processes within each stage, for instance using specific types of concrete mix and controlled environmental conditions.
- After the peak of the heat flow, hydration degree developed significantly resulting in an increased contribution of self-desiccation in capillary pressure build-up which needs to be considered particularly in mixes with high cement content and/or a W/C ratio lower than 0.5.
- Despite the well-established positive effects of curing on the mechanical properties of concrete, the results obtained demonstrate that a longer duration of sealed curing results in increased capillary pressure values of SCC without SRA. Longer curing duration increases the distribution of finer porosities and hydration degree leading to further self-desiccation and consequently higher capillary pressure value. These findings enable the determination of an application-specific optimum curing duration based on the priority of durability and/or mechanical properties of SCC.
- Using SRA reduced the capillary pressure in concrete significantly by modifying the surface tension of the pore solution. The results also indicate the improved performance of SRA due to 8 and 16 hours of curing times among which mix with 8 h of sealed curing experienced the lowest capillary pressure value confirming the better performance of SRA in the finer and semi-saturated porosities.

CRediT authorship contribution statement

Armin Jamali: Conceptualization, Methodology, Data curation, Investigation, Writing – original draft, Visualization. **Joao Mendes:** Conceptualization, Methodology, Funding acquisition, Supervision. **Brabha Nagaratnam:** Methodology, Validation, Writing – review & editing. **Michael Lim:** Methodology, Resources, Writing – review & editing.

Declaration of competing interest

The authors declare that they have no known competing financial interests or personal relationships that could have appeared to influence the work reported in this paper.

Data availability

Data will be made available on request.

Acknowledgements

The financial contribution of the Northumbria University Faculty of Engineering and Environment and the Northumbria University Department of Mechanical and Construction Engineering MCE QR Steering Funds are greatly acknowledged.

The technical support from Phil Donnelly (Senior Technician) for the manufacture of HCT components, saturation vessels and other experimental equipment necessary to conduct the experimental program.

References

[1] M.D. Cohen, J. Olek, W.L. Dolch, Mechanism of plastic shrinkage cracking in Portland cement and Portland cement-silica fume paste and mortar, Cem. Concr. Res. 20 (1) (1990) 103–119.
[2] D. Ravina, R. Shalon, Plastic shrinkage cracking, J. Proc. (1968) 282–292.
[3] M. Kayondo, R. Combrinck, W. Boshoff, State-of-the-art review on plastic cracking of concrete, Constr. Build. Mater. 225 (2019) 886–899.
[4] M. Otieno, M. Alexander, H.-D. Beushausen, Corrosion in cracked and uncracked concrete–influence of crack width, concrete quality and crack reopening, Mag. Concr. Res. 62 (6) (2010) 393–404.
[5] A. Akhavan, F. Rajabipour, Quantifying the effects of crack width, tortuosity, and roughness on water permeability of cracked mortars, Cem. Concr. Res. 42 (2) (2012) 313–320.
[6] W.P. Boshoff, R. Combrinck, Modelling the severity of plastic shrinkage cracking in concrete, Cem. Concr. Res. 48 (2013) 34–39.
[7] A.S. Goudie, Dust storms and human health, in: R. Akhtar (Ed.), Extreme Weather Events And Human Health: International Case Studies, Springer International Publishing, Cham, 2020, pp. 13–24.
[8] A. Bagheri, A. Jamali, M. Pourmir, H. Zanganeh, The influence of curing time on restrained shrinkage cracking of concrete with shrinkage reducing admixture, Adv. Civ. Eng. Mater. 8 (1) (2019) 596–610.
[9] M.J. Oliveira, A.B. Ribeiro, F.G. Branco, Shrinkage of self-compacting concrete.A comparative analysis, J. Build. Eng. 9 (2017) 117–124.
[10] M.J. Oliveira, A.B. Ribeiro, F.G. Branco, Curing effect in the shrinkage of a lower strength self-compacting concrete, Constr. Build. Mater. 93 (2015) 1206–1215.
[11] F. Sayahi, M. Emborg, H. Hedlund, A. Cwirzen, Plastic shrinkage cracking of self-compacting concrete: influence of capillary pressure and dormant period, Nordic Concr. Res. 60 (1) (2019) 67–88.
[12] F. Sayahi, M. Emborg, H. Hedlund, A. Cwirzen, Effect of admixtures on mechanism of plastic shrinkage cracking in self-consolidating concrete, ACI Mater. J. 117 (5) (2020) 51–59.
[13] T. Xie, C. Fang, M.M. Ali, P. Visintin, Characterizations of autogenous and drying shrinkage of ultra-high performance concrete (UHPC): an experimental study, Cem. Concr. Compos. 91 (2018) 156–173.
[14] S. Ghourchian, M. Butler, M. Krüger, V. Mechtcherine, Modelling the development of capillary pressure in freshly 3D-printed concrete elements, Cem. Concr. Res. 145 (2021), 106457.
[15] F. Wittmann, On the action of capillary pressure in fresh concrete, Cem. Concr. Res. 6 (1) (1976) 49–56.
[16] A. Radocea, A Study on the Mechanism of Plastic Shrinkage of Cement-based Materials, Chalmers University of Technology, 1992.
[17] A. Radocea, A model of plastic shrinkage, Mag. Concr. Res. 46 (167) (1994) 125–132.
[18] I. Löfgren, O. Esping, O. Jensen, P. Lura, K. Kovler, Early age cracking of self-compacting concrete, in: Int. RILEM Conf. Vol. Chang. Hardening Concr. Test. Mitigation" Lyngby, 2006, pp. 251–260.
[19] V. Slowik, M. Schmidt, R. Fritzsch, Capillary pressure in fresh cement-based materials and identification of the air entry value, Cem. Concr. Compos. 30 (7) (2008) 557–565.
[20] V. Slowik, T. Hübner, M. Schmidt, B. Villmann, Simulation of capillary shrinkage cracking in cement-like materials, Cem. Concr. Compos. 31 (7) (2009) 461–469.
[21] S. Ghourchian, M. Wyrzykowski, P. Lura, The bleeding test: a simple method for obtaining the permeability and bulk modulus of fresh concrete, Cem. Concr. Res. 89 (2016) 249–256.
[22] R. Combrinck, L. Steyl, W.P. Boshoff, Interaction between settlement and shrinkage cracking in plastic concrete, Constr. Build. Mater. 185 (2018) 1–11.
[23] R. Combrinck, W.P. Boshoff, Typical plastic shrinkage cracking behaviour of concrete, Mag. Concr. Res. 65 (8) (2013) 486–493.
[24] P. Lura, B. Pease, G.B. Mazzotta, F. Rajabipour, J. Weiss, Influence of shrinkage-reducing admixtures on development of plastic shrinkage cracks, ACI Mater. J. 104 (2) (2007) 187.
[25] S. Ghourchian, M. Wyrzykowski, M. Plamondon, P. Lura, On the mechanism of plastic shrinkage cracking in fresh cementitious materials, Cem. Concr. Res. 115 (2019) 251–263.
[26] V. Slowik, M. Schmidt, Early age cracking and capillary pressure controlled concrete curing, Adv. Cem. Based Mater. 126 (2010) 229–234.
[27] C. Qiao, W. Ni, J. Weiss, Transport due to diffusion, drying, and wicking in concrete containing a shrinkage-reducing admixture, J. Mater. Civ. Eng. 29 (9) (2017) 04017146.
[28] D.-Y. Yoo, N. Banthia, Y.-S. Yoon, Effectiveness of shrinkage-reducing admixture in reducing autogenous shrinkage stress of ultra-high-performance fiber-reinforced concrete, Cem. Concr. Compos. 64 (2015) 27–36.
[29] G. Sant, A. Eberhardt, D. Bentz, J. Weiss, Influence of shrinkage-reducing admixtures on moisture absorption in cementitious materials at early ages, J. Mater. Civ. Eng. 22 (3) (2010) 277–286.
[30] D. Bentz, M.R. Geiker, K.K. Hansen, Shrinkage-reducing admixtures and early-age desiccation in cement pastes and mortars, Cem. Concr. Res. 31 (7) (2001) 1075–1085.
[31] B. Rongbing, S. Jian, Synthesis and evaluation of shrinkage-reducing admixture for cementitious materials, Cem. Concr. Res. 35 (3) (2005) 445–448.
[32] J. Mora-Ruacho, R. Gettu, A. Aguado, Influence of shrinkage-reducing admixtures on the reduction of plastic shrinkage cracking in concrete, Cem. Concr. Res. 39 (3) (2009) 141–146.
[33] H. Rahoui, I. Maruyama, M. Vandamme, J.-M. Pereira, M. Mosquet, Impact of an SRA (hexylene glycol) on irreversible drying shrinkage and pore solution properties of cement pastes, Cem. Concr. Res. 143 (2021), 106227.
[34] ACI308R-16, Guide to External Curing of Concrete, American Concrete Institute, United States, 2016.
[35] V. Slowik, M. Schmidt, D. Kässler, M. Eiserbeck, Capillary pressure monitoring in plastic concrete for controlling early-age shrinkage cracking, Transp. Res. Rec. 2441 (1) (2014) 1–5.

[36] Y. Li, J. Li, Capillary tension theory for prediction of early autogenous shrinkage of self-consolidating concrete, Constr. Build. Mater. 53 (2014) 511–516.
[37] L. Huang, J. Hua, M. Kang, F. Zhou, Q. Luo, Capillary tension theory for predicting shrinkage of concrete restrained by reinforcement bar in early age, Constr. Build. Mater. 210 (2019) 63–70.
[38] J. Zhu, R. Zhang, Y. Zhang, F. He, The fractal characteristics of pore size distribution in cement-based materials and its effect on gas permeability, Sci. Rep. 9 (1) (2019) 1–12.
[39] K. Liang, X. Zeng, X. Zhou, C. Ling, P. Wang, K. Li, S. Ya, Investigation of the capillary rise in cement-based materials by using electrical resistivity measurement, Constr. Build. Mater. 173 (2018) 811–819.
[40] F. Sayahi, M. Emborg, H. Hedlund, A. Cwirzen, M. Stelmarczyk, The severity of plastic shrinkage cracking in concrete: a new model, Mag. Concr. Res. 73 (6) (2021) 315–324.
[41] M. Schmidt, V. Slowik, Capillary pressure controlled concrete curing in pavement construction, in: Airfield And Highway Pavement 2013: Sustainable And Efficient Pavements, 2013, pp. 295–306.
[42] V. Slowik, J. Ju, Discrete modeling of plastic cement paste subjected to drying, Cem. Concr. Compos. 33 (9) (2011) 925–935.
[43] P. Lura, O.M. Jensen, K. Van Breugel, Autogenous shrinkage in high-performance cement paste: an evaluation of basic mechanisms, Cem. Concr. Res. 33 (2) (2003) 223–232.
[44] J.L. Poole, K.A. Riding, K.J. Folliard, M.C. Juenger, A.K. Schindler, Methods for calculating activation energy for Portland cement, ACI Mater. J. 104 (1) (2007) 303–311.
[45] H. Samouh, E. Rozière, A. Loukili, The differential drying shrinkage effect on the concrete surface damage: experimental and numerical study, Cem. Concr. Res. 102 (2017) 212–224.
[46] A. Ridley, J. Burland, A new instrument for the measurement of soil moisture suction, Géotechnique 43 (2) (1993) 321–324.
[47] J. Mendes, O. Buzzi, New insight into cavitation mechanisms in high-capacity tensiometers based on high-speed photography, Can. Geotech. J. 50 (5) (2013) 550–556.
[48] J. Mendes, O. Buzzi, Performance of the University of Newcastle high capacity tensiometers, in: Unsaturated Soils: Research & Applications, CRC Press, 2020, pp. 1611–1616.
[49] J. Mendes, D. Gallipoli, F. Boeck, G. Von Unold, A. Tarantino, Building the UPPA high capacity tensiometer, in: E3S Web of Conferences, 2016.
[50] BS EN 197-1, Cement - Part 1. Composition, Specifications And Conformity Criteria for Common Cements, British Standards Institution, 2018.
[51] BS 8500-2 Concrete, Complementary British Standard to BS EN 206 - Specification for Constituent Materials And Concrete, British Standards Institution, 2019.
[52] BS EN 12350-8, 2019 testing fresh concrete, in: Self-compacting Concrete - Slump-flow Test, British Standards Institution, 2019.
[53] ASTM C232, Standard Test Methods for Bleeding of Concrete, ASTM International, West Conshohocken, PA 19428-2959. United States, 2017.
[54] ASTM C403, Standard Test Method for Time of Setting of Concrete Mixtures by Penetration Resistance, ASTM International, West Conshohocken, PA 19428-2959. United States, 2017.
[55] H. Samouh, E. Rozière, V. Wisniewski, A. Loukili, Consequences of longer sealed curing on drying shrinkage, cracking and carbonation of concrete, Cem. Concr. Res. 95 (2017) 117–131.
[56] K. Van Breugel, Prediction of temperature development in hardening concrete, in: Prevention of Thermal Cracking in Concrete at Early Ages 15, 1998, pp. 51–75.
[57] L. D'aloia, G. Chanvillard, Determining the “apparent” activation energy of concrete: Ea—numerical simulations of the heat of hydration of cement, Cem. Concr. Res. 32 (8) (2002) 1277–1289.
[58] H. Kada-Benameur, E. Wirquin, B. Duthoit, Determination of apparent activation energy of concrete by isothermal calorimetry, Cem. Concr. Res. 30 (2) (2000) 301–305.
[59] A.K. Schindler, K.J. Folliard, Heat of hydration models for cementitious materials, ACI Mater. J. 102 (1) (2005) 24.
[60] S. Ghourchian, M. Wyrzykowski, P. Lura, A poromechanics model for plastic shrinkage of fresh cementitious materials, Cem. Concr. Res. 109 (2018) 120–132.
[61] Y. Xi, Z.P. Bažant, H.M. Jennings, Moisture diffusion in cementitious materials adsorption isotherms, Adv. Cem. Based Mater. 1 (6) (1994) 248–257.
[62] F. Soleilhet, F. Benboudjema, X. Jourdain, F. Gatuingt, Role of pore pressure on cracking and mechanical performance of concrete subjected to drying, Cem. Concr. Compos. 114 (2020), 103727.
[63] H. Samouh, E. Roziere, A. Loukili, Experimental and numerical study of the relative humidity effect on drying shrinkage and cracking of self-consolidating concrete, Cem. Concr. Res. 115 (2019) 519–529.
[64] F. Rajabipour, G. Sant, J. Weiss, Interactions between shrinkage reducing admixtures (SRA) and cement paste's pore solution, Cem. Concr. Res. 38 (5) (2008) 606–615.